5. A. A. Beg and A. S. Baldwin Jr., *Genes Dev.* **7**, 2064 (1993).
6. D. Thanos and T. Maniatis, *Cell* **80**, 529 (1995).
7. D. St. Johnston and C. Nüsslein-Volhard, *ibid.* **68**, 201 (1992).
8. R. Geisler, A. Bergmann, Y. Hiromi, C. Nüsslein-Volhard, *ibid.* **71**, 613 (1992); S. Kidd, *ibid.*, p. 623.
9. C. Hashimoto, K. L. Hudson, K. V. Anderson, *ibid.* **52**, 269 (1988).
10. D. S. Schneider, K. L. Hudson, T.-Y. Lin, K. V. Anderson, *Genes Dev.* **5**, 797 (1991); N. J. Gay and F. J. Keith, *Nature* **351**, 355 (1991); A. Heguy, C. T. Baldari, G. Macchia, J. L. Telford, M. Melli, *J. Biol. Chem.* **267**, 2605 (1992).
11. A. Letsou, S. Alexander, K. Orth, S. A. Wasserman, *Proc. Natl. Acad. Sci. U.S.A.* **88**, 810 (1991); C. A. Shelton and S. Wasserman, *Cell* **72**, 515 (1993).
12. G. E. Croston, Z. Cao, D. V. Goeddel, *J. Biol. Chem.* **270**, 16514 (1995).
13. We seeded 293 cells in 100-mm plates at a density of 30% and transfected them on the following day with IL-1RI expression plasmid (10 μg) (*12*) and pNeoSRαII (1 μg) containing the G418 resistance gene by the calcium phosphate precipitation method (*25*). Cells that stably incorporated transfected genes were selected with G418 (600 μg/ml) (Gibco). Ten individual colonies were cloned and expanded. IL-RI expression on the cell surface was determined by fluorescence-activated cell sorting (FACS) analysis with antibody to IL-1RI. Four clones that showed adequate levels of IL-1RI expression were adapted to suspension culture in CO_2-independent minimum essential medium (MEM, Mediatech) supplemented with 10% fetal bovine serum, glucose (4.5 g/ml), 1 mM sodium pyruvate (Gibco), streptomycin (100 μg/ml), and penicillin (100 μg/ml).
14. The 293 IL-1RI cells were sedimented at 500*g* for 5 min and resuspended in serum-free MEM medium (50×10^6 cells/ml). The cells were treated with recombinant human IL-1β (200 ng/ml, Genentech) for 3 min at 37°C and sedimented at 500*g* for 5 min at 4°C. All subsequent steps were done at 4°C. Cells were suspended in five volumes of lysis buffer [50 mM Hepes (pH 7.9), 250 mM NaCl, 5 mM dithiothreitol (DTT), 1 mM EDTA, 20 mM β-glycerophosphate, 5 mM *p*-nitrophenyl phosphate, 1 mM sodium orthovanadate, 1 mM benzamidine, 0.4 mM phenylmethylsulfonyl fluoride (PMSF), 1 mM sodium metabisulfite, leupeptin (10 μg/ml), aprotinin (10 μg/ml), 0.1% NP-40, and 10% (v/v) glycerol]. After incubation on ice for 30 min with occasional rocking, the cell lysate was centrifuged at 2000*g* for 10 min. Supernatants were collected and centrifuged at 125,000*g* for 2 hours. Supernatants were stored at −70°C.
15. First-dimensional electrophoresis was isoelectrofocusing. The tube gel preparation and running conditions were described previously [O'Farrell, *J. Biol. Chem.* **250**, 4007 (1975)]. A pH gradient was created with ampholines pH 5.0 to 7.0 and pH 3.5 to 9.5 (Pharmacia) blended at a ratio of 1:1. Second-dimensional separation was achieved with 7% SDS–polyacrylamide gel electrophoresis (SDS-PAGE).
16. After thawing, the extracts were centrifuged at 125,000*g* for 2 hours. Supernatants were incubated with 35 mg of rabbit immunoglobulin G (IgG) raised to IL-1RI (*12*) and protein A–Sepharose CL4B beads (25 ml) (Pharmacia) for 4 hours at 4°C with rocking. The beads were collected in a glass Econo-column (Bio-Rad), washed with 250 ml of wash buffer 1 [50 mM Hepes (pH 7.9), 250 mM NaCl, 5 mM DTT, 1 mM EDTA, 0.1% NP-40, 20 mM β-glycerophosphate, 1 mM sodium orthovanadate, 1 mM benzamidine, 0.4 mM PMSF, and 1 mM sodium metabisulfite], and resuspended in 50 ml of kinase buffer [20 mM tris-HCl (pH 7.6), 1 mM DTT, 20 mM $MgCl_2$, 20 mM β-glycerophosphate, 20 mM *p*-nitrophenyl phosphate, 1 mM EDTA, 1 mM sodium orthovanadate, 1 mM benzamidine, 0.4 mM PMSF, 1 mM sodium metabisulfite, 5 μM unlabeled ATP, and 100 μCi of [γ-^{32}P]ATP)]. The phosphorylation reaction was incubated at 30°C for 15 min and was then incubated with unlabeled ATP (100 μM) for 15 min. The protein A beads were collected and washed sequentially with 150 ml of wash buffer 1, 150 ml of wash buffer 2 [50 mM Hepes (pH 7.9), 1 M NaCl, 5 mM DTT, 1 mM EDTA, and 0.1% NP-40] and 150 ml of wash buffer 3 [50 mM Hepes (pH 7.9), 100 mM NaCl, 2 M urea, 5 mM DTT, 1 mM EDTA, and 0.1% NP-40)]. Proteins that remained bound were eluted with 50 ml of the elution buffer (buffer 3 with 7 M urea) overnight at 4°C with rocking. The eluted material was loaded onto a 0.5-ml Q Sepharose column. After they were washed extensively with the elution buffer, proteins bound (including pp100) were eluted with 1.5 ml of the elution buffer with 0.5 M NaCl. The eluate was concentrated in a Microcon 50 (Amicon) to 50 μl, diluted with 1 ml of isoelectrofocusing sample buffer (*15*), concentrated again to 50 μl, and then subjected to 2D gel electrophoresis.
17. J. Hou *et al.*, *Science* **265**, 1701 (1994).
18. S. Hanks and A. Quinn, *Methods Enzymol.* **200**, 38 (1991); S. Hanks and T. Hunter, *FASEB J.* **9**, 576 (1995).
19. T. Hirayama and A. Oka, *Plant Mol. Biol.* **20**, 653 (1992); T. V. Moran and J. C. Walker, *Biochim. Biophys. Acta* **1216**, 9 (1993).
20. G. B. Martin *et al.*, *Science* **262**, 1432 (1993).
21. Y. L. Ing, I. W. Leung, H. H. Heng, L. C. Tsui, N. J. Lassam, *Oncogene* **9**, 1745 (1994).
22. R. L. Galindo, D. N. Edwards, S. K. Gillespie, S. A. Wasserman, *Development* **121**, 2209 (1995).
23. The IRAK coding sequence was inserted in a bacterial T7 expression vector pRSETA (Invitrogen), in fusion with a sequence encoding a polyhistidine tag. Recombinant IRAK was made in *Escherichia coli* strain BL21 induced with 1 mM isopropyl-β-D-thiogalactopyranoside, and then purified under denaturing conditions on a nickel column (Qiagen). Purified protein was used for generating antibodies in rabbits (Zymed).
24. J. Großhans, A. Bergmann, P. Haffter, C. Nüsslein-Volhard, *Nature* **372**, 563 (1994).
25. F. M. Ausubel *et al.*, *Current Protocols in Molecular Biology* (Wiley, New York, 1994), p. 9.1.1.
26. A. P. Feinberg and B. Vogelstein, *Anal. Biochem.* **132**, 6 (1983).
27. Cells were collected by centrifugation in 5 ml of phosphate-buffered saline with 1 mM EDTA, washed once with medium (10 ml), sedimented, resuspended in 1 ml of medium, and transferred to 1.5-ml microtubes. IL-1β (200 ng/ml) was added to the tubes, followed by incubation at 37°C for the indicated time. The cells were collected by centrifugation and then lysed with 1 ml of lysis buffer (*14*). After incubation on ice for 30 min, the cell debris was sedimented in a microcentrifuge and discarded. The IL-1RI complexes were immunoprecipitated (*12*), resolved by SDS-PAGE, and transferred to nitrocellulose membrane, which were blotted with antiserum to IRAK.
28. We thank D. Goeddel and S. McKnight for inspiration, support, and scientific advice; S. Wasserman for pointing out the sequence similarity in the NH_2-terminal regions of IRAK and Pelle; A. Ashkenazi for providing IL-1RI expression plasmids; A. Bothwell for pNeoSRαII; K. Williamson for nucleotide sequencing; L. Xu and S. Wong for technical support; and V. Baichwal, M. Rothe, and U. Schindler for critical review of the manuscript.

4 October 1995; accepted 8 December 1995

TECHNICAL COMMENTS

How Much Solar Radiation Do Clouds Absorb?

Anomalous absorption of solar radiation by clouds is said to exist (*1*, *2*) because shortwave absorption inferred from solar flux measurements often exceeds theoretical prediction. R. D. Cess *et al.* (*3*) suggest that solar absorption in clouds is not only significantly larger than the model prediction, but also much larger than inferred by previous measurements, including those that originally suggested the anomaly.

Current understanding predicts that absorption of solar radiation by the entire atmospheric column containing clouds is only slightly enhanced over absorption by an equivalent clear sky column. Theory predicts that cloud absorption can exceed 20% of incoming radiation (*4*) and that this absorption occurs in place of rather than in addition to clear sky absorption. Significant absorption by cloud thus does not imply anomalous absorption, and the data collected in an aircraft in the study by Pilewskie and Valero (*5*, *6*), when averaged, is actually consistent with current understanding. Thus, neither report (*3*, *5*) indicates that cloud absorption (as opposed to the total column absorption) is actually enhanced.

Measurement of atmospheric absorption is difficult to make, as it requires measurement of all radiation flowing into and from a volume. In measurements made from aircraft (*3*, *5*), the volume is ill-defined, and measurement of fluxes on its boundaries is by necessity limited to just a few locations. The usual approach is to measure the fluxes at the cloud top and base along the flight line of the aircraft and to make assumptions about the representativeness of these measurements to the unsampled regions. Given these assumptions, absorption then results as a (usually small) residual of the differences in these fluxes. When error analyses of this approach is considered, the combination of undersampling of boundary fluxes and the natural variability of the real atmosphere is too great to produce credible results (*2*, *7*). This variability results in spuriously large positive and negative excursions-to-absorption calculated as a flux difference (*8*). Where the study by Cess *et al.* (*3*) differs from others is that the above-cloud flux data derive from satellite observations, whereas the surface measurements are obtained from either a single radiometer or a network of 11 radiometers. This analysis is supposed to account for large space and time scale variability and is supposed to accommodate undersampled boundary fluxes. The report (*3*) does not contain an error analysis and or evidence to support this assumption.

Cess *et al.* introduce an approach to the

analyses of these flux data [figure 1 in (3)] which expresses the fluxes at cloud top (represented as an albedo along the y axes) as a function of downward fluxes below cloud (expressed here as a transmittance along the x axis) (9). The slope β, they argue, is governed by absorption, and estimate its value to be -0.59, which is significantly different from a slope deduced by state-of-the-art radiative transfer models (10). Although the slopes characterizing the model results vary according to where clouds occur in the atmosphere [or more precisely, how much water vapor exists above clouds (4)], the relationships shown are similar to the model results quoted by Cess *et al.* (3). The purpose of the model results shown is not to highlight differences in the slope parameter β (as in Fig. 1), but to emphasize the implications for spectral albedo of the results of Cess *et al.* (as in Fig. 2). If their analyses are assumed to be correct, then it is unclear why our present understanding is so badly flawed and why other measurements are wrong.

The cloud absorption anomaly as posed by Cess *et al.* contradicts results from other data sets. Absorption of solar radiation in the troposphere including in clouds occurs largely in the near infrared (NIR) portion of the spectrum (4) (at wavelength λ longer than about 0.7 μm). If it is supposed that the enhancement occurs in the NIR region (11), then it is simple to estimate the magnitude of the change in NIR albedo (unlike absorption, reflection is a quantity that is measurable) that is required to produce the value β found by C95. This change (Fig. 2A) is a function of transmission and indicates that a reduction of radiation of 50 to 60% is needed to account for a value of β equal to -0.59 (cloud absorption in this case is more than doubled). Existing measurements of NIR albedo, a fundamentally more accurate measure than any residual estimates of absorption (2), do not support this kind of anomaly (Fig. 2B).

The reflection of NIR radiation from clouds is detected over a narrow band of wavelengths where absorption is small (but not negligible), that is, where the change in albedo (and absorption) must be greatest (in so-called windows) (Fig. 3, y axis). A corresponding reflection at visible wavelengths is where absorption is thought to be nonexistent (Fig. 3, x axis). The relation between these reflections depends on particle size (through particle size effects on absorption) and cloud optical thickness—a dependence successfully used to remotely sense cloud particle size (12). A 50% reduction of *nir* reflection leads to a change in the estimated particle size from 10 μm, typical of the droplet size if marine water clouds to 50 μm. This is consistent neither with the demonstrated capabilities of present cloud particle size retrievals nor with known microphysics of such clouds.

Without convincing error analyses, without a reproduction of the results using different analyses and different data, and without an explanation of why other published results are inconsistent with their own, then it is difficult to evaluate the findings of Cess *et al.* (3). The nonreproducible nature of their results (3) is suggested in the results of Nemesure *et al.* (13) who analyze the same Boulder tower data and arrive at a different conclusion about the effect of clouds on the shortwave forcing. The analyses of Pilewskie and Valero [see figures 6 and 7 in (5)] also conflicts with their own "direct" measurements of absorp-

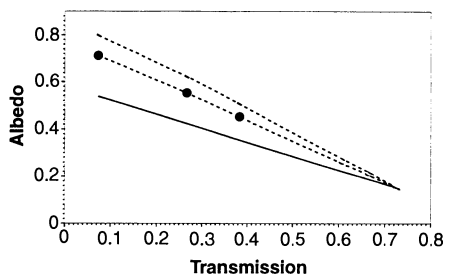

Fig. 1. Comparison of the albedo-transmission relation derived from state-of-the-art radiation models for high (---) and low (-•-) clouds contrasted to the relation shown in the report by Cess *et al.* (3). β = 0.59 (—). Units on the x and y axes are arbitrary.

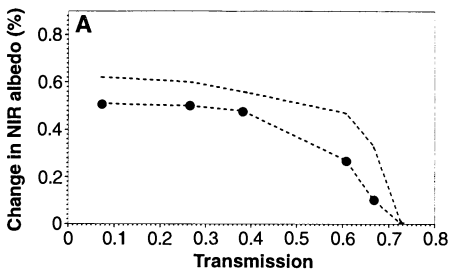

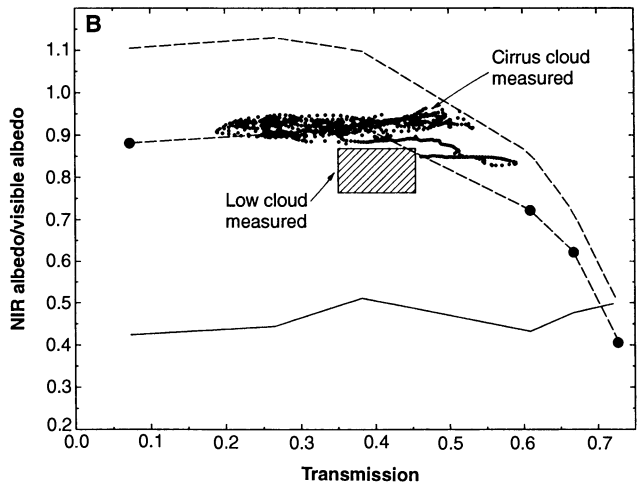

Fig. 2. (**A**) Change in NIR albedo required to bring the results of Fig. 1 into agreement with those of Cess *et al.* (**B**) Ratio of the NIR-to-visible albedo as a function of transmission. This ratio varies from 0.8 to 1.1 according to theory for transmissions less than 0.5. Direct measurements of this ratio obtained over low and high clouds are also shown. High (---) and low (-•-) clouds and β = 0.59 (—) per Cess *et al.* (3) are shown. Data identified as low cloud are from measurements reported by Hignett (12). Cirrus clouds measurements described by Smith *et al.* (13). Units on the x and y axes are arbitrary.

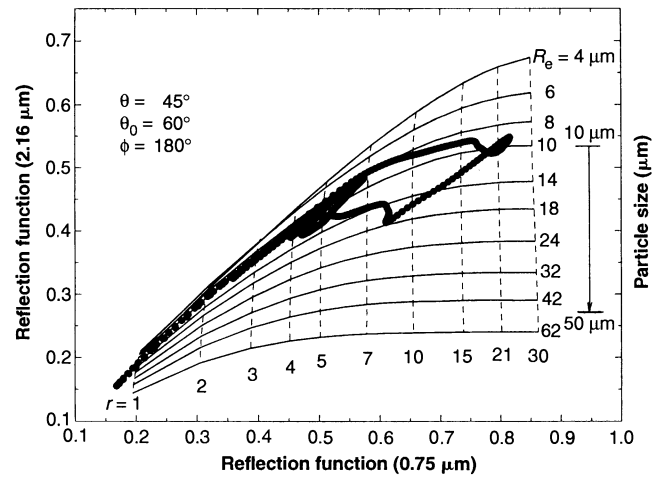

Fig. 3. NIR reflectance at 2.16 μm as a function of the 0.75 μm reflectance for a stratocumulus cloud from a 2-D radiative transfer model at a given solar-viewing geometry.

tion [figure 1 in (5)]. These results suggest that there are problems (7) with the indirect slope method used by Cess *et al.* (3). For example, the slope results in figure 6 in the report by Pilewskie and Valero (5) predicts that a cloud of 45% albedo absorbs in excess of 40% of the incident solar radiation, a result unsupported in their figure 1.

Graeme L. Stephens*
Cooperative Research Center for Southern Hemispheric Meteorology
Monash University,
Clayton, Victoria, Australia
E-mail: stephens@langley.atmos.colostate.edu

*Present address: Department of Atmospheric Science, Colorado State University, Fort Collins, CO 80523, USA.

REFERENCES AND NOTES

1. W. Wiscombe *et al.*, *J. Atmos. Sci.* **41**, 1336 (1984).
2. G. L. Stephens and S.-C. Tsay, *Q. J. R. Meteorol. Soc.* **116**, 671 (1990).
3. R. Cess *et al.*, *Science* **267**, 496 (1995).
4. G. L. Stephens, *J. Atmos. Sci.* **35**, 2111 (1978); S. Twomey, *ibid.* **33**, 1087 (1976); R. Davies *et al.*, *ibid.* **41**, 2126 (1984).
5. P. Pilewskie and F. Valero, *Science* **267**, 1626 (1995).
6. One can convert the flux difference measurements in the report by Pilewskie and Valero [figure 3 of (5)] to a fractional flux difference, which they would interpret as the fractional absorption. The mean values of the "absorption" would then range from approximately from 10% to 14%, which is entirely in keeping with theory. For reasons noted below (8), more significance should be attached to average values than to individual values [given in figure 2 of (5)].
7. This conclusion prompted other investigators to devise different ways of measuring absorption. An example is that of M. King *et al.* [*J. Atmos. Sci.* **47**, (1990)] who show slight discrepancies between theory and observation, but which is of a nature discussed by Stephens and Tsay (2) and does not support the results of Cess *et al.* (3).
8. T. Hayasaka *et al.*, *J. Appl. Meterol.* **34**, 1047 (1995). It is a typical practice to average the data in a effort to remove these spurious effects. Correction methods have also been developed, for example, by S. A. Ackerman and S. K. Cox [*ibid.* **20**, 1510 (1981)], to account for the spurious effects of undersampling solar fluxes around clouds. Correction methods were not used by Pilewskie and Valero (5).
9. A significant problem of the analyses by Cess *et al.* (3) is the assertion that reflection is a function of transmission. At absorbing wavelengths this assumption is wrong. The scattering and absorbing processes responsible for the measured albedo occur largely in the upper part of the cloud. Transmission depends on how these processes take place and not the other way around. It is more appropriate, at least on physical grounds, to consider transmission as a function of reflection (although even this is also not entirely correct). If the data of figure 6 of (5) are refitted with the dependent variables flipped, a slope of −0.82 results (which agrees with theory to the extent that the slope method is sensible). We use the model of Q. Fu and K. N. Lioa [*J. Atmos. Sci.* **50**, 2008 (1993)].
10. Theory predicts little solar absorption in the visible portion of the spectrum. Cess *et al.* imply that absorption of visible light by aerosol is unlikely to be the culprit, as they find similar anomalous values of β from flux data obtained in clean air masses over Cape Grim, Tasmania, Australia, where the relative cleanness of the air and its chemistry is well documented.
11. T. Nakajima *et al.*, *J. Atmos. Sci.* **48**, 728 (1991). There is a slight discrepancy between retrieved particle size and measured particle size. The retrieved particle sizes are typically a few microns larger than measured and explanation of the discrepancy has been elusive. It is, however, not close to the difference implied by the results of Cess *et al.* (3).
12. S. Nemesure *et al.*, *J. Climate* **7**, 579 (1994). D. Imre, personal communication.
13. P. Hignett, *Q. J. R. Meteorol. Soc.* **113**, 1011 (1987).
14. W. L. Smith Jr. *et al.*, *Mon. Weather Rev.* **118**, 2389 (1990).

5 May 1995; revised 8 May 1995; accepted 7 July 1995

Response: Stephens reflects a traditional viewpoint in stating that cloud "absorption occurs in place of rather than in addition to clear sky absorption." This is why theoretical cloud radiative transfer models predict roughly the same clear-sky and cloudy-sky (all-sky) solar absorption. But independent studies by Ramanathan *et al.* (1), Cess *et al.* (2), and Pilewskie and Valero (3) indicate that real clouds (or clouds plus atmosphere) absorb more solar radiation than do models. Stephens interprets the data in the report by Cess *et al.* (2) with the use of an atmospheric radiation model that adopts conventional plane-parallel clouds. He implements into this model a wavelength-dependent enhanced cloud absorption without adequate explanation; there are an infinite number of ways this calculation could be done, with probably infinite possible conclusions.

Stephens states that a "significant problem of the analysis by Cess *et al.* is the assertion that reflection is a function of transmission," which refers to the albedo versus transmittance regression. But as was demonstrated (2) for the Boulder-GOES data (obtained from the Geostationary Operational Environmental Satellite), the regression analysis was consistent with a direct determination of shortwave (SW) cloud-radiative forcing at the surface, $C_s(S)$, and at the top of the atmosphere, $C_s(TOA)$. This produced $C_s(S)/C_s(TOA) = 1.46$, a value that is in agreement with 1.41 from the regression analysis. Similar $C_s(S)/C_s(TOA)$ values were obtained in the other studies (1–3). In contrast, theoretical models produce $C_s(S)/C_s(TOA) \approx 1$, and this difference can only be explained by the models underestimating cloudy-sky absorption relative to clear-sky absorption (1–3).

Cess *et al.* (2) adopted the regression analysis for two reasons. First, only surface insolation was available at the other sites so it was not possible to directly determine $C_s(S)$. Second, the regression analysis did not require clear-sky identification of the surface measurements, which was difficult to determine for some data. But it is a simple task to demonstrate [in a manner analogous to what was done for the Boulder-GOES data, and using data for which we can confidently identify clear surface measurements (4)] that the regression analysis is consistent with an alternate treatment of TOA and surface measurements. With α denoting the TOA albedo and T the atmospheric transmittance (surface insolation divided by TOA insolation), it is straightforward to show that

$$\Delta\alpha/\Delta T = -(N-N_c)/(I-I_c) \quad (1)$$

where N is the net downward SW radiation at the TOA, I is the surface insolation, and N_c and I_c refer to clear-sky conditions. One can compare $\Delta\alpha/\Delta T$ (Fig. 1) as evaluated from regressions to that determined from Eq. (1), which addresses the issue of temporal and spatial sampling errors raised by Stephens. Equation 1 requires only that such errors be random so that they average to zero when evaluating the numerator and denominator of Eq. 1. The α versus T regression, however, explicitly requires all errors to be in the satellite measurements; if they were in the surface measurements, then a T versus α regression would be required, and $\Delta\alpha/\Delta T$ would be increased by the factor $1/R^2$, where R is the correlation coefficient. Sampling errors are attributable to the satellite measurements as demonstrated by the agreement between Eq. 1 and $\Delta\alpha/\Delta T$ as evaluated from the α versus T regression (Fig. 1). If it were more appropriate, as Stephens suggests, to consider T as a function of α, then Eq. 1 should agree with $\Delta\alpha/\Delta T$ as determined from the T versus α regression. This is not the case (Fig. 1), except for Oklahoma, where the large R makes the choice of the regression immaterial.

The reason that sampling errors are not attributable to the surface measurements is partially a result of temporal averaging of the surface measurements. Sampling errors occur because the satellite pixel measurements are instantaneous and over a grid that is much larger than the field of view of an upward facing pyranometer. For example, a single isolated cloud could significantly impact the surface measurement while having little impact on the satellite measurement; the reverse would occur if there were clouds over most of the satellite grid, but not over the surface instrument. But cloud systems move, so that temporally averaging the surface measurements is equivalent to spatially averaging them over the satellite grid. The Oklahoma data demonstrate this point: The regression R

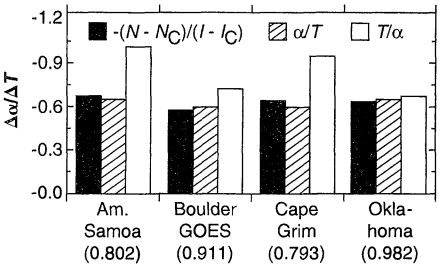

Fig. 1. $\Delta\alpha/\Delta T$ determined from Eq. 1, from an α versus T regression, and from a T versus α regression, for four geographically diverse locations. Correlation coefficients are indicated at bottom.

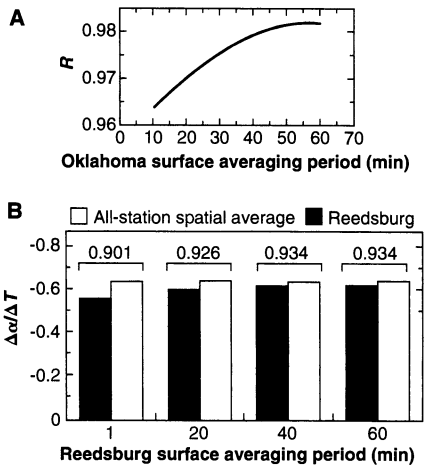

Fig. 2. (**A**) α versus T correlation coefficients (Oklahoma) as a function of the surface averaging period, which constitutes an average of the near-instantaneous surface measurements temporally centered about the time of the instantaneous satellite measurements. (**B**) $\Delta\alpha/\Delta T$ for a single station (Reedsburg) of the Wisconsin pyranometer network as a function of the surface averaging period at that site and as determined by spatially averaging the entire 11 stations within the network. All-station spatial averages adopt 1-minute surface averages and are invariant to the Reedsburg averaging period. The Reedsburg correlation coefficients are shown, and $R = 0.962$ for the all-station spatial average.

is a maximum for a surface averaging period of roughly 60 minutes (Fig. 2A), which is the averaging period used for that data. The Wisconsin data (*2*) directly demonstrate equivalence between temporal and spatial averaging. The surface measurements are from a network of 11 pyranometers located within a roughly 0.8° × 0.8° grid. The data are available as 1-minute means, and when spatially averaged over all stations the resulting $\Delta\alpha/\Delta T$ is comparable to that for a single station (Reedsburg) when the single-station measurement has been temporally averaged (Fig. 2B). For the other sites the surface measurements were available as 1-hour (American Samoa and Boulder) or half-hour (Cape Grim) means, and these temporal averages should minimize spatial sampling errors associated with the surface measurements as is consistent with Fig. 1A.

The issue raised by Stephens concerning undersampling of boundary fluxes is an argument often applied to aircraft measurements of an isolated cloud and refers to radiation escaping from the sides of the cloud that is not captured by the instruments above and below that cloud. Thus the cloud "appears" to absorb excess SW radiation because of this loss of unmeasured energy. But this isolated-cloud argument is not appropriate to our satellite-surface measurements, nor to the aircraft measurements made by Pilewskie and Valero (*3*), both of which refer to cloud systems. A study

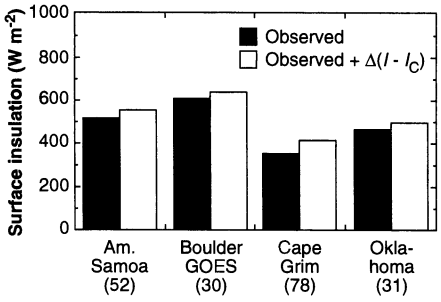

Fig. 3. Difference between $I - I_c$ for CCM2 versus the observed quantity in relation to the dayside-mean observed surface insolation. The numbers in parentheses under each site name represent $\Delta(I - I_c)$, Wm^{-2}. These data refer to dayside means and thus represent the measurement signal, in contrast to 24-hour means that are appropriate for energy budget considerations.

using a three-dimensional cloud model (*5*) concluded that the "simulation suggests that the shortwave absorptance of inhomogeneous clouds can be evaluated reasonably by means of appropriate spatial average." The point is that the "large positive and negative excursions-to-absorption" discussed by Stephens compensate when spatial averaging (*3*) or temporal averaging (*2*) is performed.

Differences between the current observations and models (as demonstrated in Fig. 3 with reference to version 2 of the National Center for Atmospheric Research Community Climate Model) are large and constitute a signal in excess of uncertainties associated with the measurements (*6*). These model-versus-observational differences, $\Delta(I - I_c)$, were evaluated so that $N - N_c$ for CCM2 was constrained to that of the observations, thus removing differences in the TOA radiation budget. The $I - I_c$ comparison also isolated cloud effects by removing model-versus-observational differences in clear-sky insolation. This comparison indicates that the model's clouds are underpredicting cloud SW absorption by overestimating cloudy-sky surface insolation relative to clear skies; we see no other plausible explanation. For the four locations, this amounts to an average surface-insolation overestimate by the traditional model of nearly 10% (Fig. 3).

R. D. Cess
M. H. Zhang
Institute for Terrestrial and Planetary Atmospheres, Marine Sciences Research Center, State University of New York, Stony Brook, NY 11794–5000, USA

REFERENCES AND NOTES

1. V. Ramanathan *et al.*, *Science* **267**, 499 (1995). In this report, the surface cloud-radiative forcing was determined as a residual of other components of the surface energy budget. A comparable value was recently determined from direct radiometric observations (D. E. Waliser, W. D. Collins, S. P. Anderson, *Geophys. Rev. Lett.*, in press).
2. R. D. Cess *et al.*, *Science* **267**, 496 (1995).
3. P. Pilewskie and F. P. J. Valero, *ibid.*, p. 1626.
4. For this purpose three data sets described by Cess *et al.* (*2*) have been used: American Samoa, Boulder-GOES, and Cape Grim. The Boulder-GOES clear-sky determination was as described earlier (*2*) and was consistent with an alternate procedure utilizing GOES clear-sky identification at the TOA. The instantaneous GOES measurements were every half-hour, and the temporally colocated hourly mean surface measurements were identified as clear if GOES identified the satellite grid as clear for the three consecutive half-hourly measurements that coincided with the hourly-mean surface measurements. For American Samoa and Cape Grim, the clear-sky identification was from the instantaneous satellite measurements for the TOA and from an upper envelope of the insolation measurements, as in (*2*), for the surface. This required normalizing both TOA and surface measurements to a mean sun-Earth distance. For our present purposes the 3-year (1985–1987) American Samoa data were extended to 5 years (1985–1989), and a data processing error that affected the original data for December 1986 and throughout 1987 was corrected. Also recent data from Oklahoma have been used; these consist of colocated GOES, TOA, and surface measurements made from 5 to 27 April 1994 as part of the Atmospheric Radiation Measurements (ARM) program. The instantaneous GOES satellite measurements were hourly, and the surface insolation measurements were near instantaneous—every 15 s. The satellite measurements were averages over a 0.3° × 0.3° grid centered at the surface instrument. The surface measurements were identified as clear if GOES identified the entire grid as clear at the time of the surface measurement.
5. T. Hayasaka *et al.*, *J. Appl. Meteorol.* **34**, 1047 (1995).
6. As discussed by Cess *et al.* (*2*), the data were taken at sites where extensive attention was given to the surface instruments in terms of calibration. Also, the results shown in Fig. 1 eliminate calibration errors and long-term drifts through differencing. There are, however, other uncertainties associated with converting satellite-measured radiances to fluxes, but these uncertainties are well below the measurement-model differences shown in Fig. 3. See the paper by B. R. Barkstrom, E. F. Harrison, and R. B. Lee III [*Eos* **71**, 279 (1990)].

1 May 1995; accepted 7 July 1995

Response: We address Stephens' criticisms of our report (*1*) in the order in which they appear in his comment. We find several errors in his arguments.

Stephens argues that 20% absorption by clouds, around the asymptotic limit predicted by theory (*2*), is in close agreement with the aircraft measurements in our report (*1*). However, our report states that (*1*) "maximum absorption approaches 30% of the solar constant" indicating, contrary to Stephens' statement, that the aircraft results are *not* consistent with current understanding. We have reproduced (Fig. 1) in units of fractional absorption, the measurements of figure 2 in our report.

Not all of the absorption by cloud occurs *in place of* (rather than in *addition to*) clear sky absorption, as Stephens suggests, but because there is considerable overlap in the absorbing bands of condensed water and water vapor, *some* cloud absorption occurs in place of clear sky absorption. We used this fact to adjust our estimate of cloud forcing ratio between the two aircraft to the

ratio that an observer on the ground would determine [note 9 in (*1*)].

Stephens refers to "the usual approach" to measure atmospheric absorption and lists the limitations of that method. But a two-aircraft technique (*3*), which was used during Tropical Ocean Global Atmosphere–Coupled Ocean Atmosphere Response Experiment (TOGA-COARE) and Central Equatorial Pacific Experiment (CEPEX) and which led to our results (*1*), eliminates the uncertainties (resulting from, in Stephens's words, "ill-defined volumes," but also from cloud advection and evolution circumstances Stephens does not mention) that plagued past aircraft studies.

In his note 8, Stephens mistakenly states that "Correction methods were not used by Pilewskie and Valero. . . ." But our report states (p. 1628) "We averaged our flux measurements over 3-min periods to smooth higher frequency features that might otherwise lead to difficulties in interpreting data sets from the two aircraft platforms." Stephens incorrectly performs an additional averaging, which artificially produces a result that he finds acceptable, in his note 6.

Error analysis by Ackerman and Cox (*5*) (cited by Stephens), shows that for 20-km cloud cells, the undersampled horizontal flux divergence at the cloud edge is 10% of the incident flux at cloud top, drops to 5% 1 km from the edge, and vanishes 2 km from the edge. The 3-min time integration in our data (*1*) translates into a 30-km path integration, sufficient to eliminate this spurious horizontal divergence effect. Furthermore, such effects depend on the scale of cloud cells and would be less (in a relative sense) for larger, more uniform cloud systems. Cloud types encountered in the tropical regions of study during TOGA-COARE and CEPEX were generally thousands of times greater (in area) than the 20 km clouds referred to by Ackerman and Cox (*5*), as evidenced by a typical tropical cloud system observed on 9 March (Fig. 2), which was comparable in size to the Australian continent.

In our report (*1*), we did not use the terminology "data correction," preferred by Stephens, because what is actually implied is an additional data-processing procedure to compensate for an incomplete theory. In this case, theory cannot account for the transfer of radiant energy from real clouds, due to an incomplete understanding of all their complexities, from the micro- to macro-physical scale. The data are indeed "correct" even if it results from cloud systems we cannot properly model. Additional processing is required to reduce the data to a state conforming to a model we can understand. The 3-min integration we applied in (*1*) had an identical effect as the procedures applied in the studies cited by Stephens (*4*, *5*), that is, it reduced the spurious effects due to horizontal flux divergence. The equality of such procedures is clearly stated in (*4*, p. 1052), "The Monte Carlo simulation suggests that shortwave absorptance of inhomogeneous clouds can be evaluated reasonably by means of appropriate spatial averaging." The basis for any "correction" is actually to enforce energy conservation principles, a much safer approach than deriving a correction based on a theoretical upper limit of cloud absorption. The elimination of such spurious effects is evident in figure 1 or figure 2 in our report, where all data points lie above the zero axis, and in figure 1 in (*1*), where there is no spurious flux data. These should have been the first clues that those points represented averages; of course, the discussion in our report (*1*) explicitly mentioned this fact.

Stephens makes the argument (in his reference 7 and in the text where he states NIR albedo is measured more accurately than integrated solar absorption) that multispectral, narrow-band measurements are more effective than net broad-band flux measurements for determining cloud absorption. However, the relative accuracy of net flux versus NIR albedo is debatable, as some flux divergences we reported (*1*) were on the order of hundreds of watts per square meter, considerably more than the "residual" anticipated by Stephens. Furthermore, what one should compare is not albedo versus absorption (that is, flux divergence), but absorption versus absorption. The retrieval of absorption from reflection (albedo) measurements requires an inverse procedure, inherently less accurate than direct observation.

Another problem with this argument is that Stephens compares broad-band to spectral data, but one should be cautious of extending the results of his figure 3, where measurements were made in bands accounting for about 0.5% of the available solar energy, to the entire solar spectrum. Although the magnitude of the absorption "anomaly" in NIR bands has been well documented (*6*), that magnitude cannot be extrapolated throughout the solar spectral region without the necessary observations in the bands where most of the solar energy

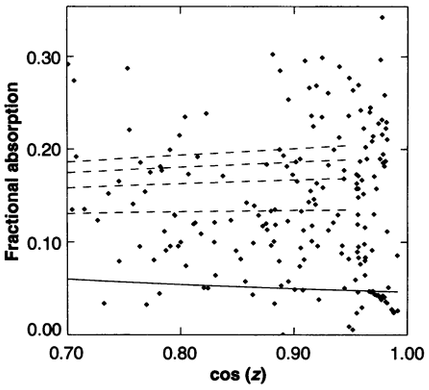

Fig. 1. Fractional cloud absorption (during TOGA-COARE and CEPEX) determined by normalizing the measured flux divergence in a 10 km to 20 km layer [figure 2 in (*1*)] by the measured incident solar flux at 20 km. Dashed curves are computed absorption for cloud thicknesses of, from top to bottom, 8, 2, 1, 0.5 km, and clear sky, with 8 km representing an asymptotic limit; from Twomey, 1976 (*2*). The solid curve is the measured clear-sky absorption in the 10- to 20-km layer.

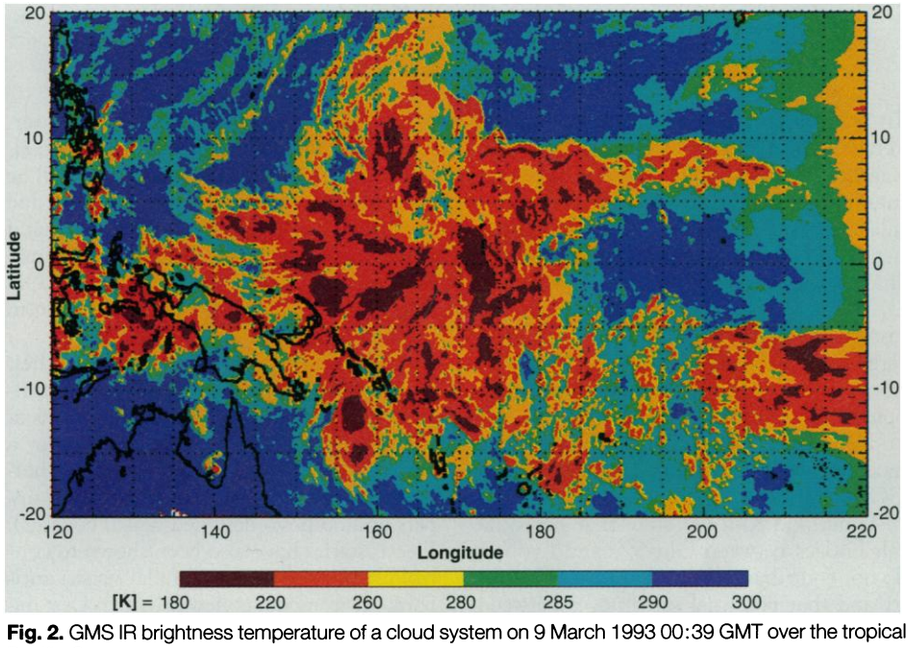

Fig. 2. GMS IR brightness temperature of a cloud system on 9 March 1993 00:39 GMT over the tropical Pacific Ocean.

is absorbed in the atmosphere, the NIR water vapor bands.

Thus, we see no way of defending Stephen's statement that conclusions based on broad-band measurements (*1*) are inconsistent with other existing data sets where discrepancies were found to occur between measurements in spectral bands and theory. Instead, the broad-band solar absorption findings presented in our report (*1*) are entirely consistent with existing spectral data sets, as both show cloud absorption to be greater than the magnitude predicted by theory.

Stephens makes another critical error when determining cloud absorption with the use of results shown in figure 6 of our report (*1*). Stephens determined cloud absorption, A, from the relationship $A + R + T = 1$, where R is reflectance and T is transmission, and he states that figure 6 in our report (*1*) indicates that a cloud with reflectance (albedo) 0.45 would absorb 0.40. His error is in assuming A occurs entirely in cloud. He does not account for the absorbing surface or for the lower 10 km of the atmosphere as well. An appropriate relationship between R and A is $R + A = 1$, where A now is the fractional absorption by the combined atmosphere-surface system (*7*). The analysis shown in figure 6 in our report is not by itself sufficient to determine cloud absorption; again we would refer the reader to figure 2 in our report (or Fig. 1 here). Consequently, contrary to Stephens erroneous conclusion, in our report (*1*) figure 1 is entirely consistent with figure 6 in our report, as those figures represent alternative ways of viewing the same data. The underlying theme is that observations cannot be reconciled with theory, regardless of the units or method of formulating cloud absorption.

Peter Pilewskie
Ames Research Center,
National Aeronautics
and Space Administration,
Mail Stop 245-4,
Moffet Field, CA 94035-1000, USA
E-mail: pil@ra.arc.nasa.gov
Francisco P. J. Valero
Scripps Institution of Oceanography,
University of California
at San Diego,
La Jolla, CA 92093, USA
E-mail: fvalero@ucsd.edu.

REFERENCES AND NOTES

1. P. Pilewskie and F. P. J. Valero, *Science* **267**, 1626 (1995).
2. S. Twomey, *J. Atmos. Sci.* **33**, 1087 (1976); G. L. Stephens, *ibid.* **36**, 2111 (1978).
3. The new approach to measure atmospheric absorption during TOGA-COARE and CEPEX evolved from a decade long airborne radiation measurement program; see F. P. J. Valero *et al.*, *Appl. Opt.* **21**, 831 (1982); *Geophys. Res. Lett.* **10**, 1184 (1983); *ibid.* **11**, 465 (1984).
4. T. Hayasaka *et al.*, *J. Appl. Meteorol.* **34**, 1047 (1995).
5. S. A. Ackerman and S. K. Cox, *ibid.* **20**, 1510 (1981).
6. G. L. Stephens and S. Tsay, *Q. J. R. Meteorol. Soc.* **116**, 671 (1990).
7. The effects of our observations beneath cloud being at 10 km instead of at the surface were discussed in our report (*1*) and shown to be consistent with the results of Cess *et al.* (*8*).
8. R. D. Cess *et al.*, *Science* **267**, 496 (1995).

1 May 1995; accepted 7 July 1995

Interhelical Salt Bridges, Coiled-Coil Stability, and Specificity of Dimerization

In their report (*1*), Kevin J. Lumb and Peter S. Kim address the contribution to the stability of the GCN4 leucine zipper of interhelical salt bridges between ionizable side chains at positions **e** and **g** in the heptad repeat denoted *gabcdef* (residue i in chain 1 with residue i′ + 5 in chain 2, **g** to **e′**). With the use of ^{13}C–nuclear magnetic resonance spectroscopy (NMR), they measured the pK_a (where K_a is the acidity constant) values of two pairs of Glu side chains potentially involved in interhelical salt bridges with Lys side chains in a synthetic model of the homodimeric leucine zipper of GCN4 (GCN4-p1).

Lumb and Kim (*1*) state that potential salt bridges between $Glu^{22,22'}$ and $Lys^{27',27}$ do not contribute to the stability of GCN4-p1 and that potential salt bridges between $Glu^{20,20'}$ and $Lys^{15',15}$ are destabilizing relative to alternative neutral-charge interactions. They conclude that i to i′ + 5 interhelical salt bridges will not necessarily contribute favorably (and in some cases will be unfavorable) to coiled-coil stability and dimerization specificity. They suggest that if there was a favorable electrostatic interaction in the folded GCN4-p1, the pK_a of Glu side chains should have been lower than in the unfolded form.

Lumb and Kim's interpretation of their results is not consistent with the experimental findings that charged side chains at these positions have been shown to play a key role in dimerization specificity (heterodimer formation) of Fos-Jun leucine zippers and de novo designed coiled coils (*2*). Electrostatics have also been shown to control chain orientation (parallel versus antiparallel) in model coiled coils (*3*). Destabilization of homodimers by side chains bearing like charges at these positions is the mechanism proposed to favor heterodimer formation where potential interhelical i to i′ + 5 salt bridges can form (*2*, *3*).

Double-mutant cycle analyses carried out in our laboratory on designed coiled coils have shown that the net electrostatic contribution per interhelical Glu-Lys salt bridge is −0.4 kcal/mol (*4*) and +0.5 kcal/mol per Glu-Glu repulsion (*5*).

Because $Glu^{22,22'}$ are involved in hydrophobic interactions with $Val^{23',23}$ through their methylenes [see figure 2C of (*1*)], the solvent accessibly of the charged carboxylate should accordingly be, on a time average, lower in the folded than in the unfolded form. Therefore, in the folded form of GCN4-p1, $Glu^{22,22'}$ will likely suffer a decrease in solvation free energy (positive $\Delta\Delta G$ solvation). Unless there is strong evidence that this likely loss of solvation free energy is exactly compensated by a negative $\Delta\Delta G_{dipole}$ term or that both of these terms are equal to zero, one cannot conclude that there is no favorable contribution to the stability of GNC4-p1 from electrostatic interactions (negative $\Delta\Delta G$ int) arising from the putative salt bridges between $Glu^{22,22'}$ and $Lys^{27',27}$ on the basis of no change in the pK_a of $Glu^{22,22'}$. On the other hand, hydrophobic interactions involving $Glu^{22,22'}$ in the folded form could play a crucial role in the net electrostatic contribution of these salt bridges to coiled-coil stability. A decrease in solvation free energy of the charged carboxylates of $Glu^{22,22'}$ in the folded form could be compensated for by the formation of hydrophobic interactions (involving the methylenes of $Glu^{22,22'}$ and $Val^{23',23}$ side chains at positions **a**), leaving a net stabilization provided by purely electrostatic interactions between Glu and Lys side chains at neutral pH, as determined by double-mutant cycle analysis on de novo designed coiled coils in our laboratory (*4*).

Lumb and Kim (*1*) state that when $Glu^{20,20'}$ are replaced by Gln residues, the stability of GCN4-p1 is increased. To explain this result, they propose that Gln side chains pack more efficiently than Glu side chains at the dimer interface. This is more a consequence rather than an explanation. The solvation free energy of a neutral polar group is about 60 kcal/mol less than that of a charged group (*6*). Therefore the fact that the $Gln^{20,20'}$ analog of GCN4-p1 is more stable likely results from a significantly lower cost of solvation free energy upon packing at the dimer interface. Moreover, replacing the charged carboxylate by a neutral carboxamide group could alleviate any destabilizing interaction of the charged carboxylate with polar groups in its surrounding at the dimer interface. Both effects should allow a stronger net contribution of hydrophobic interactions at the dimer interface from hydrophobic moieties of